

# Impact Craters on Earth with a Diameter of More than 200 km: Numerical Modeling

B. A. Ivanov\*, \*\*

*Sadovsky Institute of Geosphere Dynamics, Russian Academy of Sciences, Moscow, 119334 Russia*

\**e-mail: boris\_a\_ivanov@mail.ru*

\*\**e-mail: ivanov.ba@idg.ras.ru*

Received August 26, 2023; revised March 14, 2024; accepted March 18, 2024

**Abstract**—The three largest impact craters, the remains of which have been found on Earth to date, had diameters of about 200 km immediately after formation. The search for traces of larger impact structures continues. This paper presents the results of numerical modeling of the formation of terrestrial impact craters larger than those already found. It is shown that the inferred geothermal gradient significantly influences the initial geometry of the impact melt region, which may facilitate the search for the remains of deeply eroded ancient impact structures.

**Keywords:** impact craters, meteorite impacts, equation of state, Earth, Venus, Mars

**DOI:** 10.1134/S0038094624700370

## INTRODUCTION

In recent decades, it has been established that impact structures (craters and basins) are important components of the landscape of the Moon and other terrestrial planetary bodies. Many planetary bodies have recorded very ancient impacts, while the largest terrestrial planets, such as Earth and Mars, have had traces of ancient impacts erased. On Venus, the standard model for the rate of accumulation of impact of craters gives the longest accumulation time for observed craters from 0.5 to 1 billion years. The only planet where we can use geology and geophysics to find ancient craters is Earth. Despite the mobile lithosphere and plate tectonics, more than 150 impact structures (or their remains) have been found on Earth.

Three impact structures are of particular interest—Vredefort, Sudbury, and Chicxulub. They are often called “The Big Three” or “Three of a Kind” (Grieve and Therriault, 2000). The original (“fresh”) diameter of all three structures is estimated to be about 200 km. Two structures are very ancient (Vredefort is about 2 billion years old, and Sudbury, about 1.85 billion years old). The youngest structure, Chicxulub, 65 million years old, is overlain by younger sediments. Sudbury’s structure has been subjected to severe erosion and tectonic deformation. The Vredefort structure has been eroded to a depth of 6 to 8 km, allowing previously buried levels of the crust to be studied.

The problem discussed below is what terrestrial impact structures larger than the Big Three would look like. A partial answer may be found on Venus.

The estimated impact rate of asteroids of the same size (“bolide ratio”) is approximately 0.7 of the Earth’s value (see review by Werner and Ivanov, 2015). On Venus, with an estimated global surface age of less than one billion years, ten craters with a diameter of more than 100 km and one crater with a diameter of more than 200 km are observed (crater Mead,  $D = 270$  km, Fig. 1). The height/depth scale is relative to the deepest measured point near the center of the crater. The undulating terrain around the crater limits the accuracy of depth determination to between 1 and 1.4 km. More accurate profiles based on primary radio altimeter data presented by Ivanov and Ford (1993) give approximately the same picture (see Fig. 2 by Ivanov (2005)).

The following craters in descending size have diameters of ~180 km (Isabella) and ~150 km (Meitner). Estimates of the accumulation time of all observed Venusian craters are in the intervals: (1) less than 750 Ma (McKinnon et al., 1997), (2) 200–600 Ma (Strom et al., 1994), and (3) much smaller values, ~180 ± 70 Ma (Bottke et al., 2016). The large variation of these estimates is explained mainly by the permanent improvement of models for the evolution of the orbits of crater-forming small bodies and the refinement of the ratio of the frequencies of impacts on the Moon, Earth and Venus (Werner and Ivanov, 2015). Despite these uncertainties, the presence on Venus of ten impact craters with  $D > 100$  km, formed over a period of 200 to 600 million years (Schaber et al., 1992), should correspond to the same number of impact craters accumulated over a period of 1–2 bil-

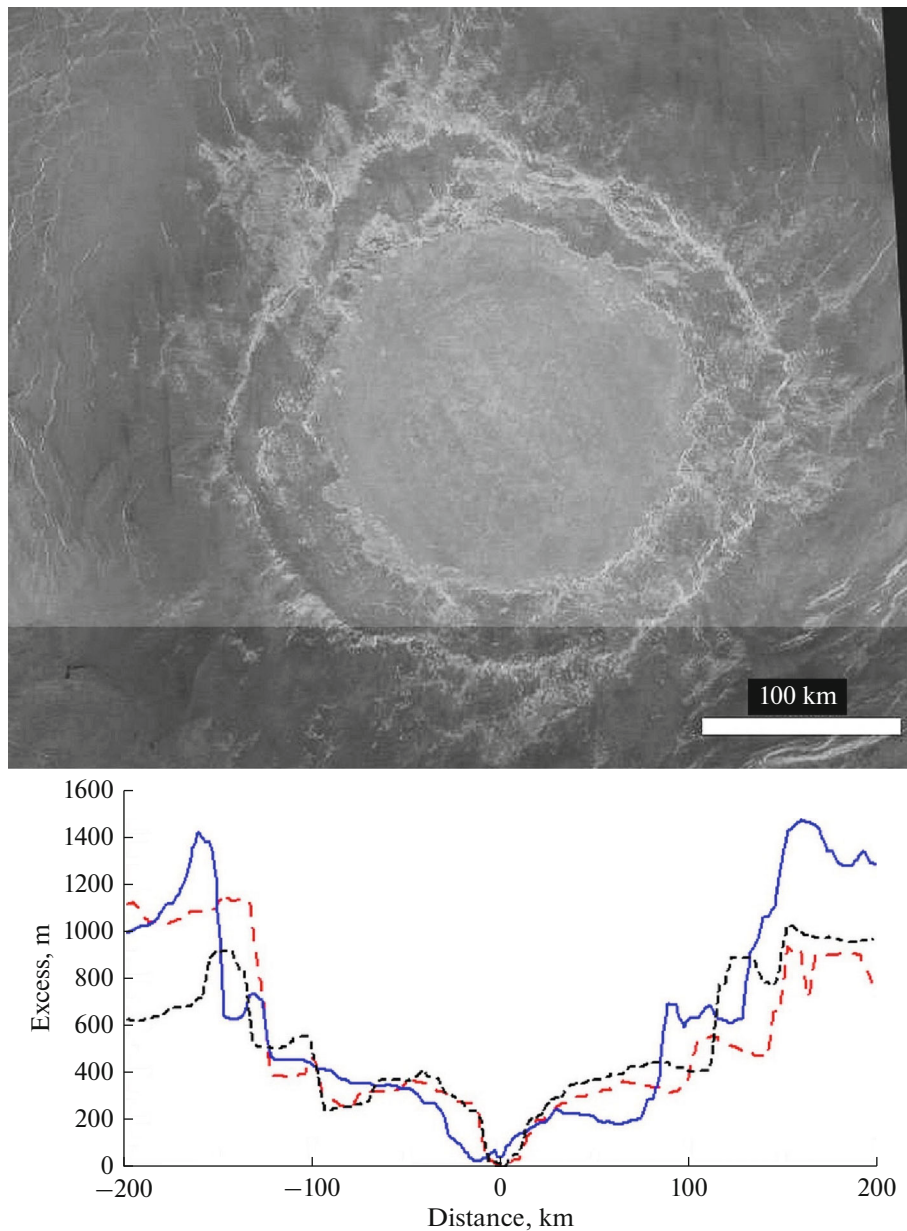


**Fig. 1.** Image of the largest known impact crater on Venus, called Mead, with a diameter  $D = 270$  km (top). Elevation profiles along three diameters (dashed, dotted, and solid curves) through Mead crater (bottom). The image and elevation profiles were constructed by the author using the publicly available JMars software (<https://jmars.asu.edu>) based on data from the *Magellan* spacecraft mission to Venus (<https://www.jpl.nasa.gov/missions/magellan/>).

lion years on the Earth's continents (considering that their area is a third of the Earth's surface). Note that for craters with a diameter of more than 100 km, the dense atmosphere of Venus can neither destroy nor slow down the projectile. It can be assumed that the rate of degradation of craters on Earth must be greater due to erosion, sedimentation and plate tectonics. However, on Earth we can find deeply eroded and buried astroblemes using modern methods of geology and geophysics.

Some idea of what preserved large impact craters look like can be obtained from images and topography

of craters on Mercury and Mars (Figs. 2, 3). However, the approximately three-times lower gravity on these planets requires additional discussion of the geometry of large craters. The crater profile on Mars (Fig. 3) has been greatly modified by younger geological processes, including the formation of younger craters, but the position of the inner ring is still noticeable. To illustrate what the initial profile of the crater might have been, the dotted line in the lower figure shows the profile of the younger and better-preserved crater Lyot ( $D \sim 200$  km) with a depth of  $\sim 4$  km, comparable to the depth of the crater on Mercury shown in Fig. 2.

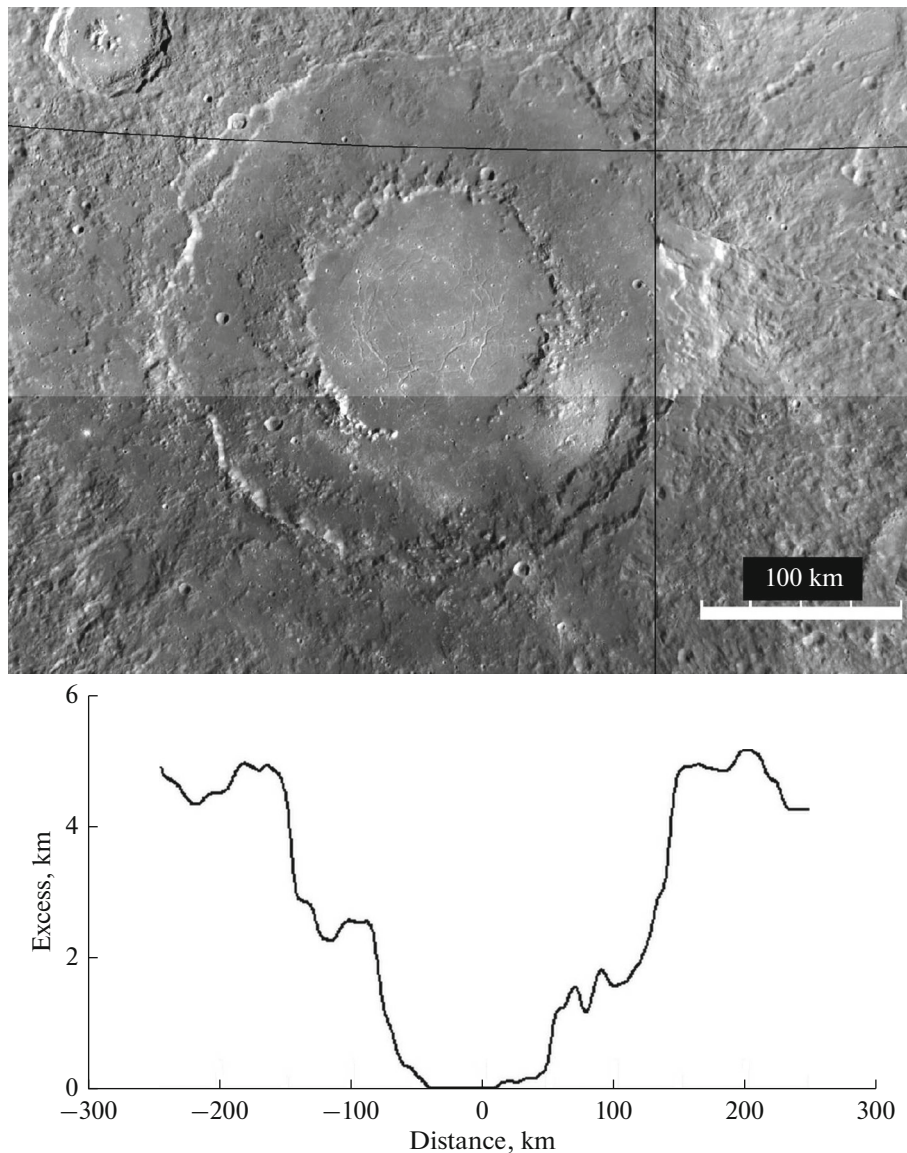


**Fig. 2.** Impact crater Rachmaninov ( $D \sim 300$  km) on Mercury (top) and the elevation profile of the surface along the diameter of the crater (bottom). The inner crater is about 4.5 km deep. The image and altitude profiles were constructed by the author using the publicly available JMars software (<https://jmars.asu.edu>) based on the results of the *Messenger* spacecraft flight to Mercury ([https://www.nasa.gov/mission\\_pages/messenger/main/index.html](https://www.nasa.gov/mission_pages/messenger/main/index.html)).

Often, the search for traces of ancient impact events includes the search for bulk deposits of multiple ejecta from craters (Simonson and Glass, 2004; Johnson and Melosh, 2012; Johnson et al., 2016; Bottke and Norman, 2017; Schulz et al., 2017; Lowe and Byerly, 2018). Less common are traces of possible individual impact events in “suspicious” areas. A study of one such site (Maniitsoq in Greenland) was proposed by Garde et al., (2012). Several years ago, the author took part in the discussion of the Garde hypothesis and carried out a small series of numerical calculations (Garde et al., 2011). Without the participation of the author, the study of the Garde hypothesis continues (Trowbridge et al., 2017). It seems to us that, more generally, regardless of the verification of the

impact origin of the Maniitsoq structure, the results of modeling large terrestrial impact structures are of interest for the search for as yet undiscovered (if they are preserved at all) ancient impact craters with a diameter greater than  $\sim 200$  km from the currently known Big Three: Vredefort, Sudbury, and Chicxulub.

## NUMERICAL MODELING

In recent years, many papers have been published on numerical simulations of large-scale impacts. This paper uses a software package known as SALEB, described in detail previously (Ivanov et al., 1997, 2010; Ivanov and Melosh, 2003; Ivanov, 2005). Fitting

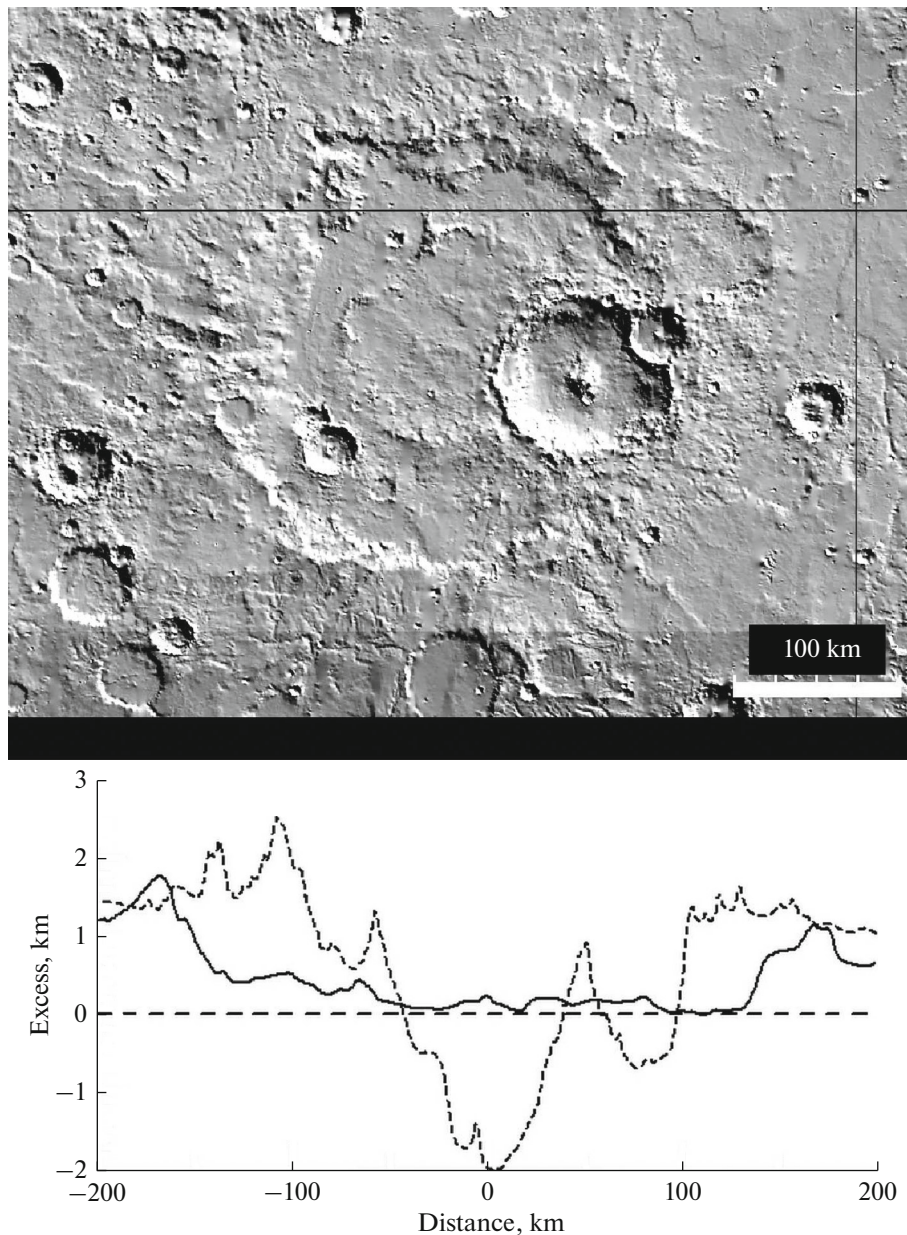


**Fig. 3.** Ancient impact crater Schröter ( $D \sim 300$  km) on Mars (top) and the altitude profile of the surface along the diameter of the crater (bottom, solid line). The dotted line shows the profile of the younger and better preserved Lyot crater (Lyot,  $D \sim 200$  km). The image and altitude profiles were constructed by the author using the publicly available JMars software (<https://jmars.asu.edu>) based on the results of several NASA spacecraft flights to Mars ([https://www.nasa.gov/mision\\_pages/mars/missions/index.html](https://www.nasa.gov/mision_pages/mars/missions/index.html)).

model parameters to best reproduction of the Big Three impact structures is described by Ivanov (2005), where field and laboratory observation data for the crater Vredefort were used to verify the model (Reimold, 1996; Gibson and Reimold, 1999; Lana et al., 2003a, 2003b). The choice of model parameters is supported by recent 2D and 3D simulations for the Chicxulub crater (Riller et al., 2018). The models of thermodynamic and strength properties of rocks in the works described above continue to be actively used in

the numerical modeling of large terrestrial craters (Allen et al., 2022; Posiolova et al., 2022; Allibert et al., 2023; Huber et al., 2023).

Because the original modeling assumed an impact structure in Greenland, current crustal thickness data (Kumar et al., 2007) were used, with corrections for possible depth of erosion using the Sudbury and Vredefort structures as examples. With a modern crust thickness of  $\sim 35$  km, options with an ancient crust thickness of up to 50 km were studied. Recent studies

by Steffen et al. (2017) give more detailed values, in southern Greenland the Mohorovičić boundary plunges from a depth of ~30 to >50 km moving from west to east.

In the following, when describing numerical modeling, we use the terminology generally accepted in papers on this topic. A tradition has developed (partly under the influence of the extensive literature on penetrating armor with a projectile) to call an impacting high-velocity body (an asteroid or comet nucleus) the term “projectile,” and the upper layers of planets or asteroids, in which an impact crater is formed, as a “target.” In this case, both the projectile and the target can have a complex structure, for example, the Earth as a target can be considered as a multilayer body consisting of spherical shells reproducing the crust, mantle, and core (see, for example, Ivanov et al., 2010).

The thermodynamic properties of the target material were described, as before, by tables calculated using the ANEOS program (Thompson and Lauson, 1972) with input parameters for granite (Pierazzo et al., 1997), basalt (Pierazzo et al., 2005), and dunite (Benz et al., 1989). Dunite modeled the mantle material, granite on top of basalt (or, for simplicity, homogeneous granite) modeled the rocks of the Earth’s crust. The assumed melting temperatures in the strength model (Collins et al., 2004) and their dependence on ambient pressure were previously described by Ivanov et al. (2010).

In the process of setting up model problems, it was found that in the case of a significant influence of melting on the crater formation process, it is necessary to pay special attention to the model melting curve of the crust and mantle and the use of an acoustic fluidization model, which will be discussed in the next section. Concluding the general description of the model, we note that most of the model options assume a vertical impact of a spherical asteroid (projectile) with a velocity  $U = 15$  km/s. For simplicity, in most versions the projectile was made of the same substance as the top layer of crust. The presented range of model options assumes projectile diameters two and four times larger than the “nominal” projectile forming the Vredefort crater—a sphere with a diameter of 12 to 14 km at an impact velocity of 15 km/s (Ivanov, 2005). These model variants are referred to as  $2 \times V$  and  $4 \times V$  for brevity.

#### MODELS USED AND VARIATION OF MODEL PARAMETERS

In most runs we use parameters of the acoustic fluidization (AF) model as proposed by Ivanov and Turtle (2001) and Ivanov and Artemieva (2002) to describe the temporary reduction of dry friction in rocks around the resulting impact crater. In some

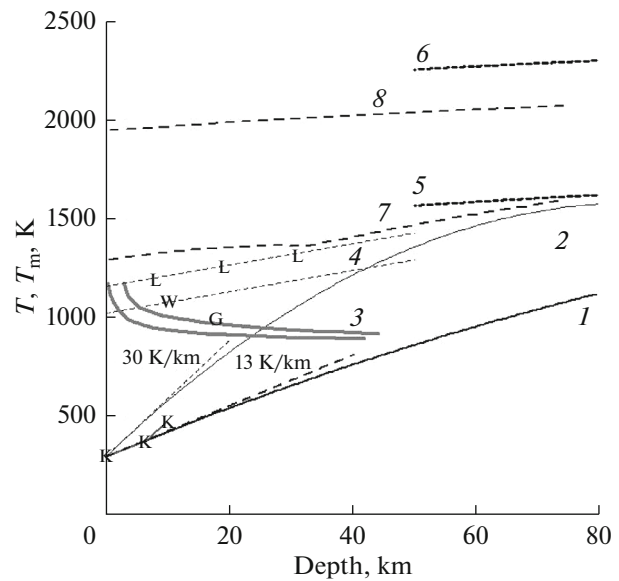


**Fig. 4.** Examples of geotherms with relatively low (1—“cold” case) and relatively high (2—“hot” case) estimated near-surface temperature gradients; 3—liquidus and solidus for water-saturated granite (Boettcher and Wyllie, 1968), “G”—experimental point from (Goetze, 1971); 4—the same for dry granite, “L”—liquidus points from (Dell’Angelo and Tullis, 1988), “W”—granite from (Rutter and Neumann, 1995). Dashed lines 4 approximate data for liquidus  $T_{liq}(K) = 1156 + 5.41z$  (km) and solidus of granite  $T_{sol} = 1020 + 5.41z$ . The “K” signs illustrate the temperature gradient in the Kola superdeep well (Popov et al., 1999). 5 and 6—Estimated solidus position for the upper mantle (5—fayalite and 6—forsterite).

model runs, we vary the selected parameters slightly, examining the model’s robustness to these variations.

The most powerful influence is the form of the inferred geotherm—how quickly the temperature of the rock increases with depth  $T(z)$  and how close the temperature  $T(z)$  approaches the melting temperature  $T_m(z)$ , which also increases with depth due to increased lithostatic pressure. To model Earth’s largest impact craters, Ivanov (2005) used a geotherm with a linear surface gradient of 13 to 15 K/km. Here we will call it a “cold” geotherm. In an attempt to reproduce the large melting zone relative to the crater, consistent with that proposed by Garde et al. (2012) for the hypothetical Maniitsoq structure, we studied the influence of possible geotherms occurring at some depth close to the melting curve  $T_m(z)$ . These several options are called “hot” geotherms here. The expected course of these geotherms and melting curves is shown in Fig. 4. Cold and hot geotherms in the case of the Moon and their influence on crater formation were discussed earlier by Ivanov et al. (2010).

Here we should make a few remarks for future improvement of the model. The computer model must describe how density, compressibility, strength/fric-

tion, and melting point change with depth. The melting temperature in such a model is important, since its value determines the disappearance of friction near the melting point. The description of the cortex as a single layer with a single function  $T_m(p)$  is still often used. To model cratering that penetrates below the crust, we need to assume an initial temperature gradient and an increase in melting temperature with increasing lithostatic pressure.

The thermal gradient in the Earth's crust varies widely due to the diversity of the mineral composition of crustal rocks (see, for example, Miller et al., 2003; Hasterok et al., 2019). Drilling of several deep wells up to 10 km in depth revealed deviations from simple thermal conductivity conditions, explained by fluid flow at unexpectedly deep levels (Popov et al., 1998). In the Kola superdeep well, the temperature gradient at depths of 5–9 km is estimated at  $\sim 20$  K/km (see Popov et al., 1998, Fig. 8.2 there). At depths  $z \sim 10$  km, the rock temperature reaches  $\sim 500$  K in the Kola well (Kukkonen and Clauser, 1994; Popov et al., 1999) and  $\sim 550$  K in the KTB well (Kontinentale Tiefbohrprogramm der Bundesrepublik Deutschland, Clauser et al., 1997).

Furlong and Chapman (2013) review the main approaches to constructing the vertical mineral and thermal structure of the Earth's crust. Temperature at the Moho boundary varies with the magnitude of heat flow, and the apparent absence of molten lower crust requires the mineral composition of the rock to change with depth, so our simple "granite" crust does not work with the typical  $T_m(p)$  for "wet granite" (Furlong and Chapman, 2013). For areas with thick crust (up to 55 km, for example in Finland), geological and geophysical analysis indicates a relatively cold asthenosphere with  $T \sim 700$  K at a depth  $z \sim 55$  km and  $T \sim 1400$  K at a depth  $z \sim 180$  km (Kukkonen, 1998). Regional variation in the mineral and thermal structure of the crust may be significant (see, e.g., Schutt et al., 2018; Puziewicz et al., 2019) and future models should be reformulated using more recent geophysical data (Cammarano and Guerri, 2017; Artemieva and Shulgin, 2019).

The mantle temperature profile is approximately modeled as an adiabat of a suitable pyrolite composition, limited by elastic wave velocities (Stixrude and Lithgow-Bertelloni, 2011). Thermal gradients in the range of 0.5 to 1 K/km seem to be a good choice to start modeling.

One of the disadvantages of the matter models most often used in calculations is the oversimplification of the description of rock melting. To correctly interpret the results, we must make some notes about possible inaccuracies.

(1) The presented modeling results have been accumulated over the past 15 years, when the ANEOS

equation of state used to construct EOS tables did not include an explicit description of melting (see for a review and ways to improve the model by Collins and Melosh (2014)). Even after recent improvements, ANEOS still describes melting in a "metallic" style: a jump in entropy at a constant temperature at a given pressure. True melting of multiminerals is a complex dynamic process. The complex behavior of the solidus and liquidus curves of crustal rocks depends on the water content in the first 50 km ( $p \sim 1.2$  GPa or  $\sim 12$  kbar), and the static solidus temperature can decrease with depth (Katz et al., 2003). The mineral composition of the material between the solidus and liquidus can change over time; experiments to determine the mineral composition of a partial melt can last from 100 to 200 h (see, for example, Pichavant et al., 2019). At high shock pressures, when rocks must melt immediately behind the shock wave front, laboratory experiments demonstrate temporary overheating of the solid (Luo and Ahrens, 2004), once again emphasizing the importance of the kinetic aspects of describing the melting of rocks and minerals. Using existing models, we can only approximately simulate rock melting as an equilibrium process.

The model used here assumes a smooth melting curve for each material,  $T_m(p)$ , with melting temperature increasing monotonically with pressure (Collins et al., 2004). In the absence of better models, we use the same value  $T_m(p)$  to estimate the decrease in rock strength as the material approaches solidus (Ohnaka, 1995). When simulating large-scale impact events, where the initial temperature increases with depth and the final position of the particle after shock compression can be located at a sufficient depth (with an elevated melting point), our simple models can only provide a qualitative illustration of crustal and mantle melting in the real Earth.

(2) Mechanical modeling of the entire crust of the Earth should include in the future a wide range of parameters that bring the description closer to the complex behavior of crustal rocks. Wet granite has liquidus and solidus temperatures that decrease with increasing pressure and water content; at a depth of 40 to 50 km, melting can occur at temperatures of  $\sim 900$  K (Goetze, 1971; Rutter and Neumann, 1995). Dehydration of the deep layers of the Earth's crust will increase the melting point. For these reasons, a thermodynamically consistent equation of state for granite suitable for computer simulations of crater formation has not yet been created. The model options in this work used a simplified description of rock melting using a single Simon curve for "ANEOS granite." Low-pressure melting temperatures ranged from  $\sim 1000$  K (dry liquidus for Westerly granite) to  $\sim 2000$  K (dry melting quartz). Figure 4 shows "hot" and "cold" model thermal profiles, in this paper distinguished by the

maximum approximation of the thermal profile  $T(z)$  to the assumed melting curve  $T_m(z)$  at depths of 20–80 km.

A similar simplified mantle model uses the ANEOS “dunite” from (Benz et al., 1989) with parameters for forsterite. From a modeling point of view, we can use the congruent melting curve for forsterite  $T_m = 2171(p/2.44 + 1)^{1/11.4}$ , proposed in (Presnall and Walter, 1993) for pressures below  $\sim 14$  GPa (this relationship is written in the style of the SALE program (see Collins et al., 2004), temperature is measured in K, pressure is measured in GPa).

Another endmember olivine composition, fayalite, melts congruently to  $\sim 6$  GPa ( $\sim 200$  km depth). Previously published experimental data can be interpolated (Akimoto et al., 1967) with the Simon equation  $T_m = 1478(p/4.1 + 1)^{1/4.8}$ .

Olivines with intermediate Mg/Fe content do not melt congruently, which is not taken into account in our simple model. In addition, model peridotites have a large difference in solidus and liquidus temperatures (Jennings and Holland, 2015). We do not yet have a simple approach to modeling the melting and mechanical properties of multicomponent rocks near the melting curve. For a preliminary search for possible effects, we vary the melt temperature at zero pressure for the model “mantle” material in the range from  $\sim 1500$  to  $2000$  K with pressure dependence  $T_m(p)$  in accordance with the experimental data given above.

In the simulation results presented here, melting point is used primarily to describe the thermal softening of rock near the solidus. For this reason, the amount of melt in our model provides only qualitative estimates of possible impact impacts on continental regions with different thermal gradients, different water contents in actual impact melts, and decreases in internal friction near the melting point, which are poorly understood for a wide range of rocks.

### SIZE OF TRANSIENT CRATER AND SCALING LAWS

To control the size of the calculated transient crater, we use the standard approach of dimensionless  $\pi$ -parameters (Schmidt and Housen, 1987), where the impact scale is specified by the parameter

$$\pi_2 = (1.61gD_{pr})/U^2. \quad (1)$$

Here  $g$  is the gravitational acceleration,  $D_{pr}$  is the diameter of the spherical projectile (or the diameter of a sphere of equal volume for nonspherical projectiles;  $D$ -projectile), and  $U$  is the impact velocity. The corresponding dimensionless parameters are the diameter  $D_{tc}$ , depth  $d_{tc}$ , and volume  $V_{tc}$  of the transient crater:

$$\begin{aligned} \pi_{D_{tc}} &= D_{tc}(\rho/m)^{1/3}, & \pi_{d_{tc}} &= d_{tc}(\rho/m)^{1/3}, \\ \text{and } \pi_{V_{tc}} &= V_{tc}(\rho/m), \end{aligned} \quad (2)$$

where  $m$  is the mass of the projectile and  $\rho$  is the effective density of the target material.

Note that in a more complete similarity theory, additional dimensionless parameters are introduced to describe the ratio of the densities of the projectile and the target and the strength parameters of the material (Holsapple and Schmidt, 1979; Schmidt and Housen, 1987; Prieur et al., 2017). In most of our calculations, the projectile consisted of ANEOS granite with an initial density of  $2.7 \text{ g/cm}^3$ .

It is important to comment on the transient crater parameters used. Although the dimensions of the transient crater can be easily extracted from the parameters of the calculation cells (for example, by tracing the position of the boundary using partially filled cells), we must take into account that the radius, depth, and volume of the transition crater we need can be achieved at different times. In this paper, a massless marker particle was placed in the initial Eulerian grid in the center of each cell, the movement of which through the computational grid was determined by the velocity vector interpolated from the velocity values at four nodes of the rectangular grid forming the cell in which the marker is located at a given time.

To some extent, the sequence in which the various parameters of the transition cavity are achieved depends on the scale of the impact event. In the model versions of this paper (transition crater with a diameter from  $\sim 80$  to  $\sim 200$  km), the maximum depth of the transition crater is first reached (20–25 s after the impact). A minor problem with determining the maximum depth is whether to consider the crater floor to be the position of the initial zero depth marker or to measure the slightly shallower depth below the surface of the deepest cell of deformed projectile material. In this paper, we typically measure the depth to the first cell on the symmetry axis containing condensed material. At the impact velocity  $U = 15 \text{ km/s}$  used here, strong evaporation does not occur for the materials used.

At the time when the transient crater reaches its maximum volume (from 60 to 80 s after the impact), the radius of the crater continues to grow. In many studies, the value of the transient crater radius used in relation (2) is fixed at the time moment of passing the maximum of the volume versus time dependence. The radius of the transient crater is determined by the vertical velocity of motion of the material at the edge of the crater at the level of the preimpact surface. We record the radius of the transient crater at the time moment when the vertical component of the velocity changes sign from upward (“ejection”) to downward (“subsidence”). This value is close to the radius of the transition crater, determined at the moment the crater volume reaches its maximum below the initial surface. In our model variants, a change in the sign of the vertical velocity is usually observed a little earlier than the

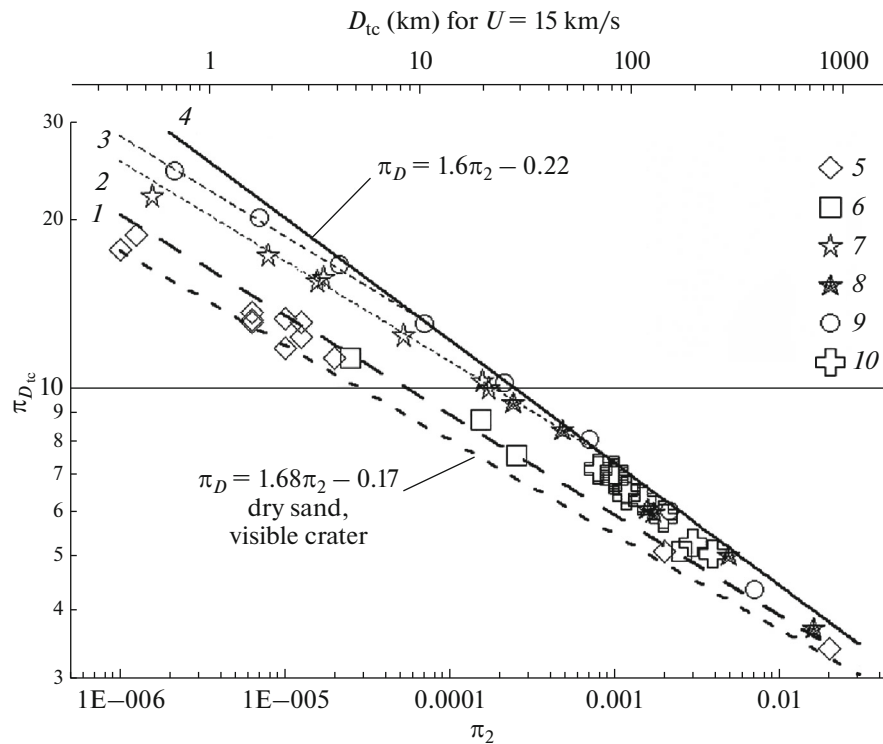


**Fig. 5.** Dimensionless diameter of the transient crater  $\pi_{D_{tc}}$  (Eq. (2)) depending on the dimensionless value of the projectile  $\pi_2$  (Eq. (1)). For clarity, the upper horizontal axis shows the diameter of the projectile (km) for earthly gravity and impact velocity  $U = 15$  km/s. The experimental dependence for dry sand (lower dotted line) is taken from (Schmidt and Housen, 1987). The approximation of the calculated data for low-velocity impacts ( $U = 5$  km/s) is shown with long dashes (1). The scaling law for a target without porosity is shown by solid line 4. The approximation of the calculated points to line 4 at high impact velocities is shown by lines 2 (impact velocity  $U = 20$  km/s) and 3 ( $U = 30$  km/s). Calculation points 5–9 are taken from modeling results for homogeneous targets with dry friction and thermal softening (Ivanov and Kamyshenkov, 2012). Calculations with a friction coefficient of 0.6 for  $U = 5$  km/s: 5—spherical projectile; 6—elliptical projectile with a thickness of half the horizontal diameter; 7—friction 0.6, ANEOS-quartzite target (Melosh, 2007),  $U = 20$  km/s; 8—friction 0.6, target—CaO (lime),  $U = 20$  km/s; 9—the same as 8, but for  $U = 30$  km/s; and 10—the present paper.

volume reaching its maximum, but in variants with the largest projectile (for example, “ $4 \times$  Vredefort,”  $4 \times V$ ), the volume maximum was reached  $\sim 30$  s earlier (60 s after impact versus 90 s to change the sign of the vertical velocity). During these 30 s, the radius of the transition crater increased from 94 to 114 km. Consequently, the discrepancy in the values of the radius (diameter) of the transition crater can be 10–15% only due to the different definition of this value.

The description of the similarity of craters in the  $\pi$ -formulation, according to Eqs. (1) and (2), turns out to be convenient only in simplified cases (homogeneous target, low strength of the substance, constant friction coefficient, etc.), when the dimensionless parameters of the transient crater (2) can be approximated by simple power-law dependences on the scale parameter  $\pi_2$  (1) in a wide range of its values. Recently, uniform material porosity and uniform material strength have been added to the set of characteristic parameters (Wunnemann et al., 2006; Elbeshausen et al., 2009; Poelchau et al., 2013; Prieur et al., 2017). In a real large-scale problem, these parameters vary with

depth, calling into question simple power-law  $\pi$  relations. Fortunately, for large terrestrial craters, variable depth porosity has little effect on crater similarity (Collins, 2014).

Any further complication of the problem (multilayered target, thermal softening of rocks, etc.) leads to a complication of the scaling laws. Ivanov and Kamyshenkov (2012) presented a number of numerical simulations over a wide range of impact velocities, from 5 to 30 km/s. If we define the “effectiveness” of mechanical impact on a target as the dimensionless depth or diameter of the transition crater by Eq. (2) at a constant value of the parameter  $\pi_2$  by Eq. (1), then we can say that impacts with low velocity are less effective than impacts with  $U \geq 15$  km/s, which is most likely due to nonlinear strength/friction effects on temperature. In general, the efficiency of high-velocity impacts tends to the limit of the scaling law for a target without porosity, strength, and internal friction at large  $\pi_2$  (Figs. 5, 6).



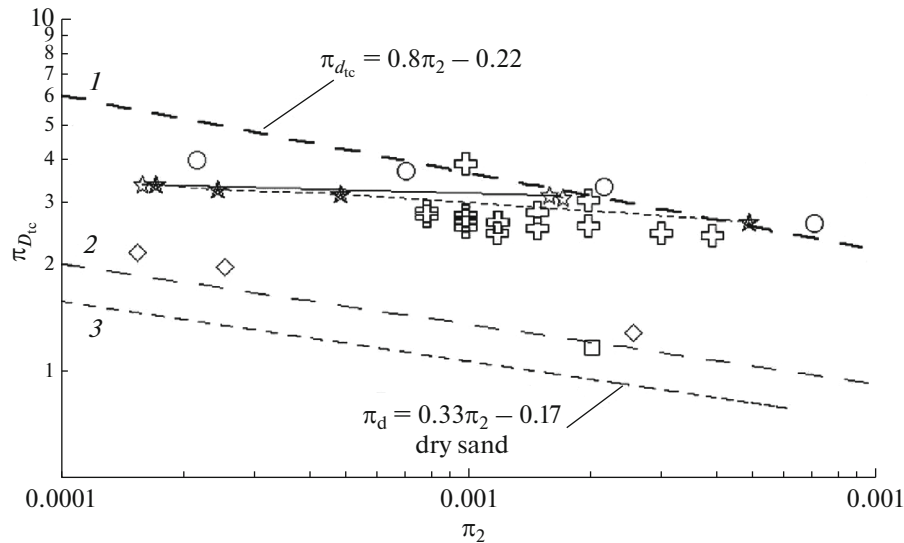


**Fig. 6.** Calculation points for the depth of the transient crater in a homogeneous target with dry friction (Ivanov and Kamysheikov, 2012) in comparison with the results of this paper. The same designations are used as in Fig. 5. 1—Generalized dependence on the depth scale of a transition crater in a homogeneous target without strength (Schmidt and Housen, 1987). 2—Calculated dependence for low-velocity impacts on a target with dry friction (Ivanov and Kamysheikov, 2012). 3—Generalized experimental dependence of the depth of craters in dry sand (Schmidt and Housen, 1987).

In this paper, the model considers a layered target (crust over mantle), where the presence of a denser underlying layer can increase the effective density of the target as the transition crater penetrates the denser mantle. After this warning, we present a plot of the model dimensionless diameter of the transition crater in Fig. 5. Dependences for the dimensionless depth of the transient crater are shown in Fig. 6 in comparison with data of Ivanov and Kamysheikov (2012).

Figures 5 and 6 show that for impacts with low velocity ( $U = 5$  km/s), the dependences of transient depths and diameters of model craters to scale on graphs with a double logarithmic scale look like approximately parallel straight lines with interpolation of experimental data for dry sand (Schmidt, 1987; Schmidt and Housen, 1987). The model craters are slightly wider and deeper than the laboratory craters in sand, since the numerical model does not take into account the porosity of the target material. The efficiency correction factor for crater diameter for porous dry sand is about 0.8: the model impact transition crater at low-impact velocity is about 20% larger than the experimental craters in porous dry sand.

Scaling laws for a medium without porosity (see Fig. 5 for diameter and Fig. 6 for crater depth) were once proposed as an extrapolation of experimental data for water-saturated sand presented in (Schmidt and Housen, 1987). The experimental scaling laws for dry sand (Figs. 5, 6) have been often cited for many years as typical scaling laws for porous targets, in contrast to the data-based relationships for wet sand, widely cited as the scaling law for nonporous rocks

with large scale impacts, where the influence of strength begins to be much less than the influence of gravity. Detailed numerical modeling in recent years has made it possible to more accurately characterize these scaling laws. For example, Nowka et al. (2010) showed how reducing porosity under constant dry friction smoothly increases the efficiency of crater formation while maintaining the same slope of the curve in double logarithmic coordinates  $\pi_D - \pi_2$ . At the same time, for zero porosity, an increase in dry friction in the target reduces the efficiency of crater formation, reducing the degree in  $\alpha$  in a typical power law of similarity  $\pi_D \sim \pi_2^{-\alpha}$  from 0.22 (low strength  $\approx$  “hydrodynamic” target) to  $\sim 0.17$  (previously the exponent for dry sand, now the exponent for a target with dry friction) (see short discussion in (Werner and Ivanov, 2015)).

In the terms described above, our calculations complement previously published data (Ivanov and Kamysheikov, 2012) and illustrate (Figs. 5, 6) a smooth transition, as the scale parameter  $\pi_2$  increases, from the “dry friction” regime to the “solid material” regime (“hydrodynamic scaling”). At the same time, it should be noted that for materials with nonlinear mechanical properties (thermal softening, variable plastic limit and friction coefficient, etc.), a simple scaling law with one exponent is not enough to assess the efficiency of crater formation. For example, data for the depth of high-velocity transition craters (Fig. 6) form an almost flat dependence  $\pi_{D_{tc}} - \pi_2$  in the range of  $\pi_2$  values from  $\sim 2 \times 10^{-5}$  to  $\sim 2 \times 10^{-3}$ , in contrast to low-velocity impacts. Of course, the scaling law for

targets with “real” models of mechanical strength should include a more complex dependence on impact velocity compared to simple power relations with the parameter  $\alpha$  equal to 0.17 or 0.22.

### COLLAPSE OF TRANSITION CRATER

The complete time sequence of the crater formation process has been described previously (see, for example, Ivanov (2005)). For the Vredefort crater, the most suitable model set of parameters for a vertical impact involves an asteroid with a diameter of 14 km and an impact velocity of 15 km/s. A shock wave propagates from the point of impact, and a transient crater begins to grow in the target material, which is mechanically damaged by the shock wave. For the model crater Vredefort, approximately 30 s after the impact, the transient crater reaches its maximum depth and begins to collapse in the gravity field. The central part of the near-crater flow is shown in Fig. 7, where the molten material is shown in red by Lagrangian tracers heated above 1700 K. In the version shown in Fig. 7, a projectile with a diameter of 14 km was used, falling vertically onto the target at a velocity 15 km/s. The calculation area is covered with an Eulerian grid with a cell size of  $0.7 \times 0.7$  km. A Lagrangian tracer is initially placed in each cell of material, which “records” the pressure, density, and temperature in the cell. Visualization of target deformation is made using black dots for every tenth row and every tenth column of the initial position of the tracers. Tracers that “recorded” temperatures of 1700 K and above are shown as red dots and roughly indicate the geometry of the melt zone (temperature above the solidus). The blue tracer chain consists of tracers that, in their final geometry, form a future erosion surface at a depth of 8 km below the initial surface level. In this version, a three-layer target model is used—the upper crust (dark gray tone), the lower crust (lighter tone), and the mantle (darker tone deeper than 50 km).

Figure 7 illustrates that the transient crater for an impact of this size (depth and diameter of about 30–40 km) is large enough for the crustal rocks to move back to the center during gravitational collapse and push up most of the impact melt that was initially “smeared” across the bottom of the transition crater. During collapse, the future horizon after impact erosion reaches its final position approximately 180 s after impact, and subsequent motion is concentrated in the collapsing central uplift (see studies of central uplift collapse in Morgan et al., 2016; Baker et al., 2016).

Using the same set of model parameters as in the crater Vredefort formation model described above, we increased the size of the projectile by a factor of 2 and 4 (the corresponding models are named  $2 \times V$  and  $4 \times V$ ), correspondingly increasing the size of the computational cell at a constant resolution of 20 CPPR

(20 cells per projectile diameter). Here a new problem for modeling arises—can we assume that the model of temporary reduction of dry friction due to acoustic fluidization (AF model, Melosh and Ivanov, 1999) works for deep mantle rocks in the same way as for crystalline crustal rocks? More generally, is our modeling experience applicable to reproducing the temporary reduction in dry friction around a nascent impact crater for deep mantle rocks at higher pressures and temperatures? Without a clear answer to this question, we started with two versions of the models—with and without the use of the AF model for mantle rocks.

The model results for options  $2 \times V$  and  $4 \times V$  are presented in Figs. 8–10. Modelling with a projectile doubled in diameter ( $2 \times V$ , Fig. 8) show the absence of impact melt in the mantle. The use of the AF model for the mantle affects the geometry of the mantle uplift, but does not affect the main result of doubling the size of the projectile—the appearance of a deep, melt-filled neck in the center of the crater.

The next doubling of the projectile size to 56 km ( $4 \times V$ ) at the same impact velocity and the same target structure leads to impact melting of the mantle and an increase in the volume of the melt “lake” in the center of the crater (Fig. 9). Here, the influence of turning on/off AF effects in the mantle material is even less noticeable than in the  $2 \times V$  variant as increased lithostatic pressure and temperature lead to plastic behavior of the mantle material even without an additional decrease in dry friction associated with acoustic fluidization.

Note that during the estimated  $\sim 1000$  s, the motion of matter in the molten zone still does not stop. And we can observe the slow gravitational separation of the molten crustal material of lower density and the denser melt of the mantle matter. For this scale of impact event, the final geometry of the melt zone will be established after prolonged thermal cooling, with possible differentiation of new rocks crystallizing from the impact melt.

In Fig. 10 we compare the profiles of model craters for the model variants shown in Figs. 8 and 9. In Fig. 10, the interval of graduating marks on the vertical axis is equal to the size of the calculation cell to emphasize the approximate nature of the obtained profiles. The final crater profile is covered by only 5–8 vertical computational cells, which leads to low spatial resolution regarding the “accurate” shape of the crater. Within the current spatial resolution limitations, we can only state that the simulated craters have a flat bottom ( $\pm 1$  cell undulations), a depth of 2 to 3 km, and a crater rim raised 2.5 to 3 km above the level of the original target surface. In general, the crater geometry obtained in the model does not contradict the available information on large impact structures on the Moon, Venus, Mars, and Mercury (Figs. 1–3). For

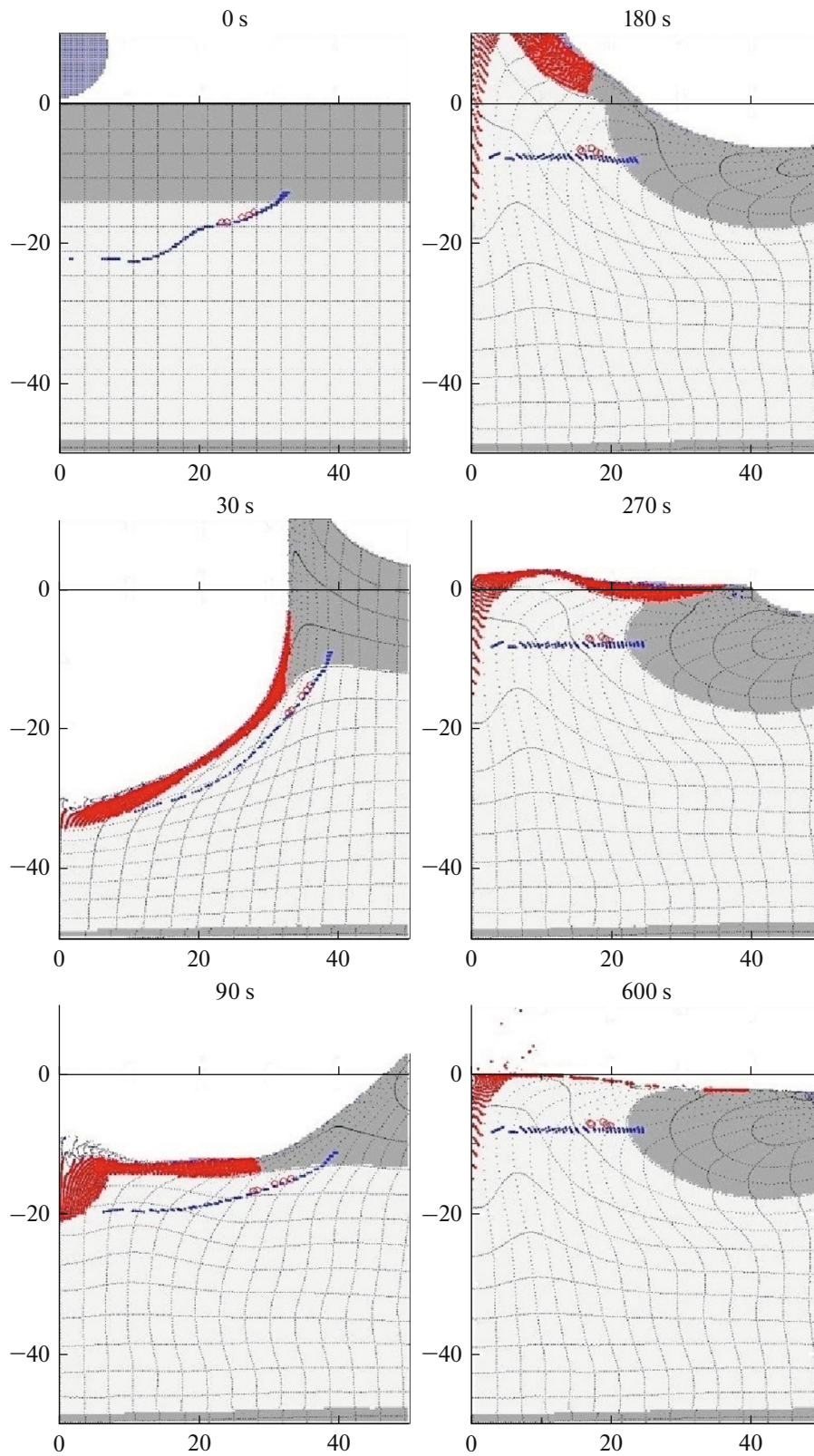


**Fig. 7.** Deformation and movement of material in the central part of a model crater on the scale of the crater Vrederfort. The distances along the axes are given in km. The time after impact is indicated above each figure.

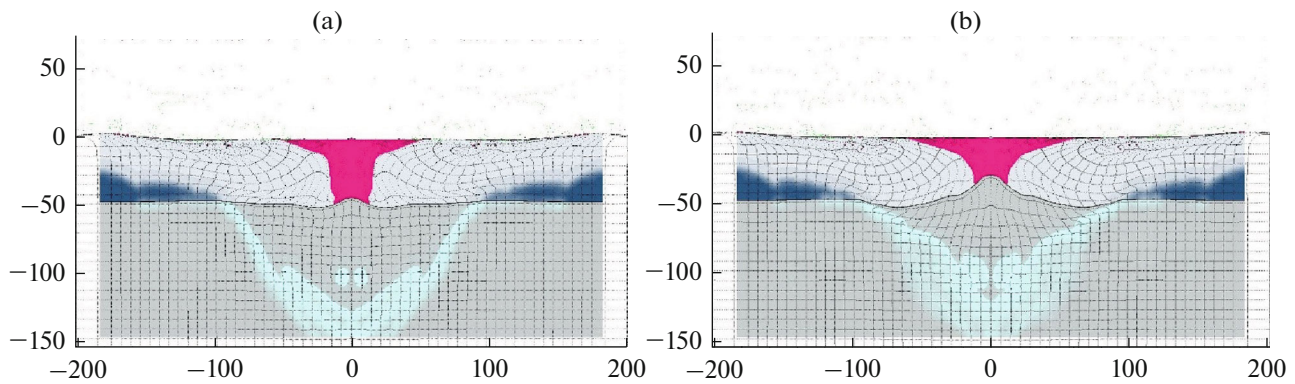


**Fig. 8.** The final ( $\sim 18$  min after impact) cross-section of the model crater for a projectile with twice the diameter (relative to the Vredefort crater projectile) (model  $V \times 2$ ,  $D_{pr} = 28$  km, and  $U = 15$  km/s), calculated without using the AF model (acoustic fluidization model) in the mantle (a) and using this model (b). The position of the impact melt is indicated in pink. Other color variations reflect different levels of rock damage (Collins et al., 2004). Horizontal and vertical distances are in km.

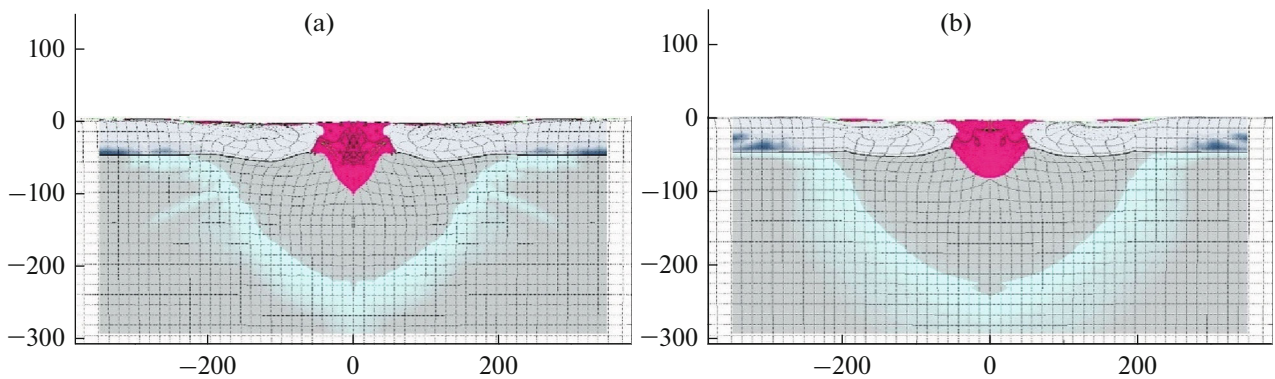


**Fig. 9.** Final ( $\sim 18$  min after impact) cross-section of a model crater for quadruple (relative to the Vredefort crater projectile) projectile diameter (denoted  $4 \times V$ ,  $D_{pr} = 57$  km, and  $U = 15$  km/s) calculated without using the acoustic fluidization model for mantle material (a) and using this model (b). Other color variations reflect different levels of rock damage (Collins et al., 2004). Horizontal and vertical distances are in km.

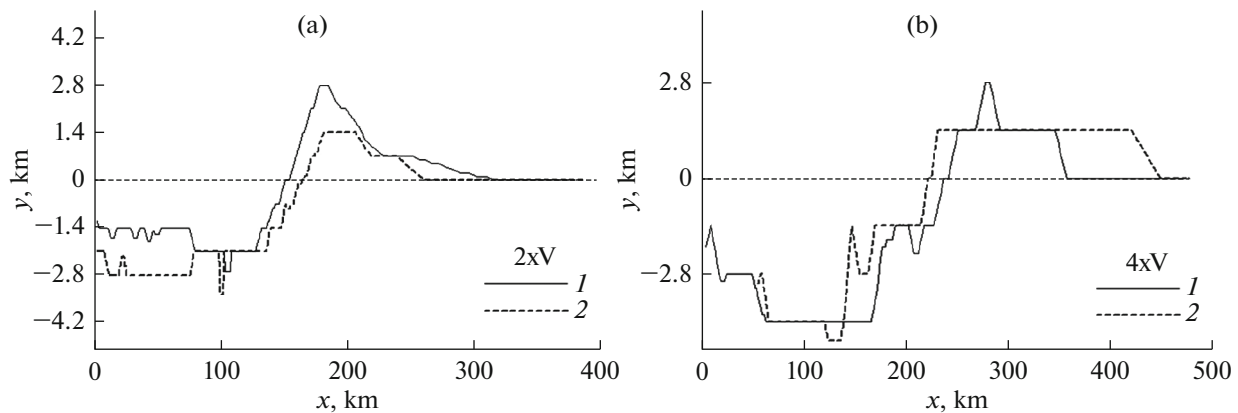


**Fig. 10.** Profiles of model craters for options  $2 \times V$  (a) and  $4 \times V$  (b) with high vertical magnification to show the relatively shallow depth ( $\sim 1.5$  and  $\sim 3$  km, respectively) of the final craters with apparent diameters of  $\sim 300$  and  $\sim 500$  km. Small graduations on the vertical axis correspond to the sizes of the calculation cells  $\Delta x = 0.7$  km ( $2 \times V$  option) and  $\Delta x = 1.4$  km ( $4 \times V$  option). The profiles in panels (a) and (b) correspond to calculations using the model of acoustic fluidization in the mantle (1) and without using it (2).

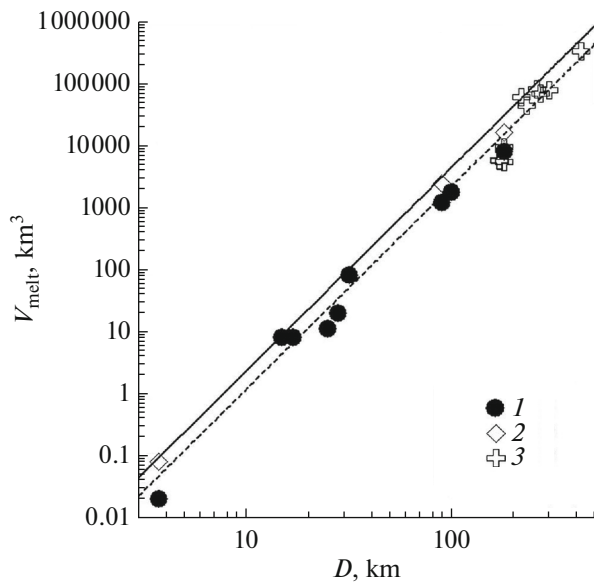


**Fig. 11.** Estimation of the volumes of impact melt in known terrestrial meteorite craters from the work (Cintala and Grieve, 1998): 1—observations, 2—maximum estimates, and 3—model results of this paper. Solid and dotted trend lines are described in the text.

Venus (and possibly other planetary bodies), the observed modern topography may differ from the model geometry immediately after the impact due to slow processes such as viscous relaxation (Karimi and Dombard, 2017).

### STRUCTURE OF THE TARGET UNDER THE CRATERS

It is believed that large eroded structures would be found on a geologically active Earth (Plado et al., 1999). Therefore, the main interest is to identify initially deep impact structures that can be exposed by erosion. The rate of erosion for the two largest impact structures (Vredefort and Sudbury) is estimated to be 6–8 km within  $\sim 2$  Ga after their formation (Ivanov, 2005). On the modern erosional cross-section we see mainly impact-altered rocks raised from initial depths of the order of  $1/10 D$  and the remains of the original impact melt basin (severely deformed by post-impact tectonics). For the  $2 \times V$  and  $4 \times V$  scale impacts studied, we gain some insight into the possible position of the impact melt, since in these cases the modeled position of the impact melt indicates a larger melt pool depth.

**Volume of melt.** In the presented simulation, we estimated the volume of the impact melt as the total volume of computational cells with a final temperature above the solidus of the target material. Some of the molten particles are ejected beyond the computational grid, some small portions of hot material are numerically “diluted” by colder material during computational advection (see discussion (Ivanov et al., 2010)).

For this reason, the numerical estimates are approximate. It is possible to compare the simulated and “measured” volumes of impact melt, as shown in Fig. 11, made on the basis of Fig. 5 from the work (Werner and Ivanov, 2015). Here, an analytical estimate of the total volume of impact melt during impacts on a crystalline target is compared with geological estimates (Cintala and Grieve, 1998) for well-studied terrestrial impact structures. The volumes of impact melt calculated for supposed terrestrial craters with  $D > 200$  km seem to be a natural continuation of the previously proposed trend  $V_{\text{melt}}(D) \approx (0.0007-0.0014) \times D^{3.3}$  (volume is in  $\text{km}^3$  and diameter is in km), where the uncertainty in the numerical coefficient reflects the possibility of ejection of part of the melt outside the central region (Werner and Ivanov, 2015).

**“Hot rod.”** Comparing model impacts with a basic scale of  $1 \times V$  ( $1 \times$  Vredefort, Fig. 7) and impacts with a twofold and fourfold increased diameter of possible projectiles ( $2 \times V$ , Fig. 8; and  $4 \times V$ , Fig. 9), we note the main observable effect: in larger craters, the uplift collapse of the transition crater floor does not push the impact melt upward, creating a shallow melt pool surrounding the central ridge in well-preserved craters such as the Boltysky crater, Ukraine (Valter et al., 1982; Grieve et al., 1987). Instead, the impact melt is “squeezed” by the rocks of the collapsing transition crater, forming a relatively narrow vertical region of molten material—a “hot stock.”

The idea of a “hot rod,” or a vertical throat filled with melt, at the center of a collapsed transition crater, was proposed by Senft and Stewart (2011) for craters on icy bodies. Our model reproduces a similar mechanism for stone bodies. When the volume of impact-molten rocks becomes comparable to the volume of the transition crater, the movement of rocks during crater collapse “captures” the impact melt near the vertical central axis and the rise of the crater bottom does not have time to push all the melt onto the surface of the central mountain, which occurs in models of the formation of craters with a diameter of  $< 200$  km. The formation of a central impact melt basin is reliably observed in simulations of lunar and Martian impact basins (Ivanov et al., 2010; Potter et al., 2012).

From the many parameters of hot rod geometry observed in the simulation, we selected the simplest parameter—the diameter of the hot rod at the assumed erosion level 20 km below the surface level at the moment of impact (Table 1). The largest craters on Venus, Mars, and Mercury show a limited range of modern depths in the range of 2–3 km. Therefore, it can be assumed that viscous relaxation of the original crater will not radically change the position of the “hot rod.”

### CONCLUSIONS

This work began many years ago in discussion with Adam Garde, who proposed an impact origin for the

**Table 1.** Model impact parameters: equivalent diameter of the spherical projectile  $D_{pr}$  ( $D$ -projectile), type of thermal gradient—cold or hot—and the main final parameters of the simulated impact structure

Calculated variant	$D_{pr}^{1)}$ , km	Thermal gradient	$D_r^{2)}$ , km	$D_a^{3)}$ , km	$W_{20}^{4)}$ , km	$d_{tc}^{5)}$ , km	$D_{tc}^{6)}$ , km
G3	32.2	Cold	360	310	40	60	150
G4	32.2	Hot	420	340	87	62	148
G5	28.2	Hot	360	280		57	132
G6	24.2	Cold	340	250	30	45	117
G7	16.1	Hot	220	180	25	34	85
G8	12.1	Hot	180	110		25	64

<sup>1)</sup> The equivalent diameter of the spherical projectile. <sup>2)</sup> The diameter of the calculated crater at the rim crest. <sup>3)</sup> The diameter of the calculated crater at the level of the original surface. <sup>4)</sup>  $W_{20}$  is the diameter of the central body of the impact melt in the central stock at a depth of 20 km below the level of the initial target surface. <sup>5)</sup> The transient cavity depth. <sup>6)</sup> The transient cavity diameter.

Maniitsoq structure in Greenland (Garde et al., 2011, 2012). Recent studies by Yakymchuk et al. (2021) argue against an impact origin of this structure. However, the question of the possibility of detecting terrestrial impact structures with a diameter of more than 200 km and an age of more than 2 billion years remains open. Numerical modeling predicts a long-lived impact melt “lake” in the central part of a fairly large crater; this is partly evidenced by geological structures in the eroded Sudbury crater, Canada (Grieve and Therriault, 2000). Independent numerical simulations of the formation of terrestrial impact craters with a diameter of about 300 km (Trowbridge et al., 2017) generally confirm the results of this work. In addition, the model results are consistent with the geology of large impact craters observed on Venus, Mercury, and Mars from spacecraft. However, additional research is needed to assess the possibility of preserving the remains of terrestrial impact craters of large size and age more than 2 billion years, taking into account erosion and terrestrial tectonics.

#### FUNDING

The work was carried out within the framework of the state assignment of the Ministry of Education and Science of the Russian Federation (project no. 122032900178-7).

#### CONFLICT OF INTEREST

The author of this work declares that he has no conflicts of interest.

#### OPEN ACCESS

This article is licensed under a Creative Commons Attribution 4.0 International License, which permits use, sharing, adaptation, distribution and reproduction in any medium or format, as long as you give appropriate credit to

the original author(s) and the source, provide a link to the Creative Commons license, and indicate if changes were made. The images or other third party material in this article are included in the article’s Creative Commons license, unless indicated otherwise in a credit line to the material. If material is not included in the article’s Creative Commons license and your intended use is not permitted by statutory regulation or exceeds the permitted use, you will need to obtain permission directly from the copyright holder. To view a copy of this license, visit <http://creativecommons.org/licenses/by/4.0/>

#### REFERENCES

- Akimoto, S.-I., Komada, E., and Kushiro, I., Effect of pressure on the melting of olivine and spinel polymorph of  $Fe_2SiO_4$ , *J. Geophys. Res.*, 1967, vol. 72, no. 2, pp. 679–686.  
<https://doi.org/10.1029/JZ072i002p00679>
- Allen, N.H., Nakajima, M., Wünnemann, K., Helhoski, S., and Trail, D., A revision of the formation conditions of the Vredefort crater, *J. Geophys. Res.: Planets*, 2022, vol. 127, no. 8, p. e2022JE007186.
- Allibert, L., Landeau, M., Röhlen, R., Maller, A., Nakajima, M., and Wünnemann, K., Planetary impacts: Scaling of crater depth from subsonic to supersonic conditions, *J. Geophys. Res.: Planets*, 2023, vol. 128, no. 8, p. e2023JE007823.
- Artemieva, I.M. and Shulgin, A., Making and altering the crust: A global perspective on crustal structure and evolution, *Earth Planet. Sci. Lett.*, 2019, vol. 512, pp. 8–16.
- Baker, D.M.H., Head, J.W., Collins, G.S., and Potter, R.W.K., The formation of peak-ring basins: Working hypotheses and path forward in using observations to constrain models of impact-basin formation, *Icarus*, 2016, vol. 273, pp. 146–163.
- Benz, W., Cameron, A.G.W., and Melosh, H.J., The origin of the Moon and the single-impact hypothesis III, *Icarus*, 1989, vol. 81, no. 1, pp. 113–131.

- Boettcher, A.L. and Wyllie, P.J., Melting of granite with excess water to 30 kilobars pressure, *J. Geol.*, 1968, vol. 76, no. 2, pp. 235–244.
- Bottke, W.F. and Norman, M.D., The late heavy bombardment, *Ann. Rev. Earth Planet. Sci.*, 2017, vol. 45, pp. 619–647.
- Bottke, W.F., Vokrouhlicky, D., Ghent, B., Mazrouei, S., Robbins, S., and Marchi, S., On asteroid impacts, crater scaling laws, and a proposed younger surface age for Venus, *Lunar Planet. Sci. Conf.*, 2016, vol. 47, p. 2036.
- Cammarano, F. and Guerri, M., Global thermal models of the lithosphere, *Geophys. J. Int.*, 2017, vol. 210, no. 1, pp. 56–72.
- Cintala, M.J. and Grieve, R.A.F., Scaling impact-melt and crater dimensions: Implications for the lunar cratering record, *Meteorit. Planet. Sci.*, 1998, vol. 33, pp. 889–912.
- Clauser, C., Giese, P., Huenges, E., Kohl, T., Lehmann, H., Rybach, L., Šafanda, J., Wilhelm, H., Windloff, K., and Zoth, G., The thermal regime of the crystalline continental crust: Implications from the KTB, *J. Geophys. Res.: Solid Earth*, 1997, vol. 102, no. B8, pp. 18417–18441.
- Collins, G.S., Numerical simulations of impact crater formation with dilatancy, *J. Geophys. Res.: Planets*, 2014, vol. 119, p. 2600–2619.
- Collins, G.S. and Melosh, H.J., Improvements to ANEOS for multiple phase transitions, *Lunar Planet. Sci. Conf.*, 2014, vol. 45, p. 2664.
- Collins, G.S., Melosh, H.J., and Ivanov, B.A., Modeling damage and deformation in impact simulations, *Meteorit. Planet. Sci.*, 2004, vol. 39, no. 2, pp. 217–231.
- Dell'Angelo, L.N. and Tullis, J., Experimental deformation of partially melted granitic aggregates, *J. Metamorph. Geol.*, 1988, vol. 6, no. 4, pp. 495–515.
- Elbeshhausen, D., Wünnemann, K., and Collins, G.S., Scaling of oblique impacts in frictional targets: Implications for crater size and formation mechanisms, *Icarus*, 2009, vol. 204, pp. 716–731.
- Furlong, K.P. and Chapman, D.S., Heat flow, heat generation, and the thermal state of the lithosphere, *Ann. Rev. Earth Planet. Sci.*, 2013, vol. 41, no. 1, pp. 385–410.
- Garde, A.A., Ivanov, B.A., and McDonald, I., Beyond Vredefort, Sudbury and Chicxulub, *Meteorit. Planet. Sci. Suppl.*, 2011, vol. 74, p. 5249.
- Garde, A.A., McDonald, I., Dyck, B., and Keulen, N., Searching for giant, ancient impact structures on Earth: The Mesoarchaean Maniitsoq structure, West Greenland, *Earth Planet. Sci. Lett.*, 2012, vol. 337, pp. 197–210.
- Gibson, R.L. and Reimold, W.U., The significance of the Vredefort Dome for the thermal and structural evolution of the Witwatersrand Basin, South Africa, *Mineral. Petrol.*, 1999, vol. 66, pp. 5–23.
- Goetze, C., High temperature rheology of Westerly granite, *J. Geophys. Res.*, 1971, vol. 76, no. 5, pp. 1223–1230.
- Grieve, R. and Theriault, A., Vredefort, Sudbury, Chicxulub: Three of a kind?, *Ann. Rev. Earth and Planet. Sci.*, 2000, vol. 28, pp. 305–338.
- Grieve, R.A.F., Reny, G., Gurov, E.P., and Ryabenko, V.A., The melt rocks of the Boltysk impact crater, Ukraine, USSR, *Contrib. Mineral. Petrol.*, 1987, vol. 96, no. 1, pp. 56–62.
- Hasterok, D., Gard, M., Cox, G., and Hand, M., A 4 Ga record of granitic heat production: Implications for geodynamic evolution and crustal composition of the early Earth, *Precamb. Res.*, 2019, vol. 331, p. 105375.
- Holland, T. and Powell, R., Calculation of phase relations involving haplogranitic melts using an internally consistent thermodynamic dataset, *J. Petrol.*, 2001, vol. 42, no. 4, pp. 673–683.
- Holsapple, K.A. and Schmidt, R.M., A material-strength model for apparent crater volume, *Proc. Lunar and Planet. Sci. Conf. 10th*, New York: Pergamon Press, 1979, pp. 2757–2777.
- Huber, M.S., Kovaleva, E., Rae, A.S.P., Tisato, N., and Gulick, S.P.S., Can Archean impact structures be discovered? A case study from Earth's largest, most deeply eroded impact structure, *J. Geophys. Res.: Planets*, 2023, vol. 128, no. 8, p. e2022JE007721.
- Ivanov, B.A., Numerical modeling of the largest terrestrial meteorite craters, *Sol. Syst. Res.*, 2005, vol. 39, pp. 381–409.
- Ivanov, B.A. and Artemieva, N.A., Numerical modeling of the formation of large impact craters, in *Catastrophic Events and Mass Extinctions: Impact and Beyond*, Geological Society of America, Spec. Pap. 356, Koeberl, C. and MacLeod, K.G., Eds., Boulder, Colorado: GSA, 2002, pp. 619–630.
- Ivanov, B.A., Deniem, D., and Neukum, G., Implementation of dynamic strength models into 2D hydrocodes: Applications for atmospheric breakup and impact cratering. I, *J. Impact Eng.*, 1997, vol. 20, nos. 1–5, pp. 411–430.
- Ivanov, B.A. and Ford, P.G., The depths of the largest impact craters on Venus (abstract), *Lunar and Planet. Sci. Conf. 24*, 1993, pp. 689–690.
- Ivanov, B.A. and Kamyshenkov, D., Impact cratering: Scaling law and thermal softening, *Lunar and Planet. Sci. Conf. 43*, 2012, p. 1407.
- Ivanov, B.A. and Melosh, H.J., Impacts do not initiate volcanic eruptions: Eruptions close to the crater, *Geology*, 2003, vol. 31, no. 10, pp. 869–872.
- Ivanov, B.A., Melosh, H.J., and Pierazzo, E., Basin-forming impacts: Reconnaissance modeling, in *GSA Special Papers 465*, Gibson, R.L. and Reimold, W.U., Eds., Boulder, Colorado, USA: Geol. Soc. Am., 2010, pp. 29–49.
- Ivanov, B.A. and Turtle, E.P., Modeling impact crater collapse: Acoustic fluidization implemented into a hydrocode, *Lunar and Planet. Sci. Conf. 32*, 2001, p. 1284.
- Jennings, E.S. and Holland, T.J.B., A simple thermodynamic model for melting of peridotite in the system NCFMASOCr, *J. Petrol.*, 2015, vol. 56, no. 5, pp. 869–892.
- Johnson, B.C., Collins, G.S., Minton, D.A., Bowling, T.J., Simonson, B.M., and Zuber, M.T., Spherule layers, crater scaling laws, and the population of ancient terrestrial impactors, *Icarus*, 2016, vol. 271, pp. 350–359.
- Johnson, B.C. and Melosh, H.J., Impact spherules as a record of an ancient heavy bombardment of Earth, *Nature*, 2012, vol. 485, no. 7396, pp. 75–77.

- Karimi, S. and Dombard, A.J., Studying lower crustal flow beneath Mead basin: Implications for the thermal history and rheology of Venus, *Icarus*, 2017, vol. 282, pp. 34–39.
- Katz, R.F., Spiegelman, M., and Langmuir, C.H., A new parameterization of hydrous mantle melting, *Geochem., Geophys. Geosyst.*, 2003, vol. 4, no. 9, pp. 1–19.
- Kukkonen, I.T., Temperature and heat flow density in a thick cratonic lithosphere: The SVEKA transect, central Fennoscandian Shield, *J. Geodyn.*, 1998, vol. 26, no. 1, pp. 111–136.
- Kukkonen, I.T. and Clauser, C., Simulation of heat transfer at the Kola deep-hole site: Implications for advection, heat refraction and palaeoclimatic effects, *Geophys. J. Int.*, 1994, vol. 116, no. 2, pp. 409–420.
- Kumar, P., Kind, R., Priestley, K., and Dahl-Jensen, T., Crustal structure of Iceland and Greenland from receiver function studies, *J. Geophys. Res.: Solid Earth*, 2007, vol. 112, no. B3, pp. 1–19.
- Lana, C., Gibson, R.L., Kisters, A.F.M., and Reimold, W.U., Archean crustal structure of the Kaapvaal craton, South Africa—evidence from the Vredefort dome, *Earth Planet. Sci. Lett.*, 2003a, vol. 206, nos. 1–2, pp. 133–144.
- Lana, C., Gibson, R.L., and Reimold, W.U., Impact tectonics in the core of the Vredefort dome, South Africa: Implications for central uplift formation in very large impact structures, *Meteorit. Planet. Sci.*, 2003b, vol. 38, pp. 1093–1107.
- Lowe, D.R. and Byerly, G.R., The terrestrial record of late heavy bombardment, *New Astron. Rev.*, 2018, vol. 81, pp. 39–61.
- Luo, S.-N. and Ahrens, T.J., Shock-induced superheating and melting curves of geophysically important minerals, *Phys. Earth Planet. Inter.*, 2004, vols. 143–144, pp. 369–386.
- McKinnon, W.B., Zahnle, K.J., Ivanov, B.A., and Melosh, H.J., Cratering on Venus: Models and observations, in *Venus II*, Bougher, S.W., Hunten, D.M., and Phillips, R.J., Eds., Tucson, Arizona: Univ. Arizona Press, 1997, pp. 969–1014.
- Melosh, H.J., A hydrocode equation of state for SiO<sub>2</sub>, *Meteor. Planet. Sci.*, 2007, vol. 42, no. 12, pp. 2079–2098.
- Melosh, H.J. and Ivanov, B.A., Impact crater collapse, *Ann. Rev. Earth Planet. Sci.*, 1999, vol. 27, pp. 385–415.
- Melosh, H.J. and Ivanov, B.A., Slow impacts on strong targets bring on the heat, *Geophys. Res. Lett.*, 2018, vol. 45, no. 6, pp. 2597–2599.
- Miller, C.F., McDowell, S.M., and Mapes, R.W., Hot and cold granites? Implications of zircon saturation temperatures and preservation of inheritance, *Geology*, 2003, vol. 31, no. 6, pp. 529–532.
- Morgan, J.V., Gulick, S.P.S., Bralower, T., Chenot, E., Christeson, G., Claeys, P., Cockell, C., Collins, G.S., Coolen, M.J.L., Ferrière, L., and 28 co-authors, The formation of peak rings in large impact craters, *Science*, 2016, vol. 354, no. 6314, pp. 878–882.
- Nowka, D., Wunnemann, K., Collins, G.S., and Elbeshausen, D., Scaling of impact crater formation on planetary surfaces, *Eur. Planet. Sci. Congress*, 2010, abs. no. 87. <https://meetingorganizer.copernicus.org/EPSC2010/EP-SC2010-87.pdf>.
- Ohnaka, M., A shear failure strength law of rock in the brittle-plastic transition regime, *Geophys. Res. Lett.*, 1995, vol. 22, no. 1, pp. 25–28.
- Plado, J., Pesonen, L.J., Puura, V., Dressler, B.O., and Sharpton, V.L., Effect of erosion on gravity and magnetic signatures of complex impact structures: Geophysical modeling and applications, in *Large Meteorite Impacts and Planetary Evolution II*, Boulder, CO: Geological Society of America, 1999, pp. 229–239.
- Pichavant, M., Weber, C., and Villaros, A., Effect of anorthite on granite phase relations: Experimental data and models, *Compt. Rend. Geosci.*, 2019, vol. 351, no. 8, pp. 540–550.
- Pierazzo, E., Artemieva, N.A., and Ivanov, B.A., Starting conditions for hydrothermal systems underneath Martian craters: Hydrocode modeling, in *Spec. Paper 384: Large Meteorite Impacts III*, 2005, pp. 443–457.
- Pierazzo, E., Vickery, A.M., and Melosh, H.J., A reevaluation of impact melt production, *Icarus*, 1997, vol. 127, pp. 408–423.
- Poelchau, M.H., Kenkmann, T., Thoma, K., Hoerth, T., Dufresne, A., and Schüfer, F., The MEMIN research unit: Scaling impact cratering experiments in porous sandstones, *Meteorit. Planet. Sci.*, 2013, vol. 48, no. 1, pp. 8–22. <https://doi.org/10.1111/maps.12016>
- Popov, Yu.A., Pevzner, S.L., Pimenov, V.P., Romushkevich, R.A., and Pevzner, S.L., Geothermal characteristics of the SG-3 section, in *Kol'skaya sverkhglubokaya. Nauchnyye rezul'taty i opyt issledovaniy* (Kola Super-deep. Scientific Results and Research Experience), Laverov, N.P. and Orlov, V.P., Eds., Moscow: MF Tekhnoneftegaz, 1998, pp. 176–190.
- Popov, Y.A., Pevzner, S.L., Pimenov, V.P., and Romushkevich, R.A., New geothermal data from the Kola superdeep well SG-3, *Tectonophysics*, 1999, vol. 306, no. 3, pp. 345–366.
- Posiolova, L.V., Lognonné, P., Banerdt, W.B., Clinton, J., Collins, G.S., Kawamura, T., Ceylan, S., Daubar, I.J., Fernando, B., Froment, M., and 42 co-authors, Largest recent impact craters on Mars: Orbital imaging and surface seismic co-investigation, *Science*, 2022, vol. 378, no. 6618, pp. 412–417.
- Potter, R.W.K., Collins, G.S., Kiefer, W.S., McGovern, P.J., and Kring, D.A., Constraining the size of the South Pole-Aitken basin impact, *Icarus*, 2012, vol. 220, pp. 730–743.
- Presnall, D.C. and Walter, M.J., Melting of forsterite, Mg<sub>2</sub>SiO<sub>4</sub>, from 9.7 to 16.5 Gpa, *J. Geophys. Res.: Solid Earth*, 1993, vol. 98, no. B11, pp. 19777–19783.
- Prieur, N.C., Rolf, T., Luther, R., Wünnemann, K., Xiao, Z., and Werner, S.C., The effect of target properties on transient crater scaling for simple craters, *J. Geophys. Res.: Planets*, 2017, vol. 122, pp. 1704–1726.
- Puziewicz, J., Czechowski, L., Grad, M., Majorowicz, J., Pietranik, A., and Šafanda, J., Crustal lithology vs. thermal state and Moho heat flow across the NE part of the European Variscan orogen: A case study from SW Poland, *Int. J. Earth Sci.*, 2019, vol. 108, no. 2, pp. 673–692.



- Reimold, W.U. and Gibson, R.L., Geology and evolution of the Vredefort impact structure, South Africa, *J. African Earth Sci.*, 1996, vol. 23, no. 2, pp. 125–162.
- Riller, U., Poelchau, M.H., Rae, A.S.P., Schulte, F.M., Collins, G.S., Melosh, H.J., Grieve, R.A.F., Morgan, J.V., Gulick, S.P.S., Lofi, J., Diaw, A., McCall, N., and Kring, D.A., Rock fluidization during peak-ring formation of large impact structures, *Nature*, 2018, vol. 562, no. 7728, pp. 511–518.
- Rutter, E.H. and Neumann, D.H.K., Experimental deformation of partially molten Westerly granite under fluid-absent conditions, with implications for the extraction of granitic magmas, *J. Geophys. Res.: Solid Earth*, 1995, vol. 100, no. B8, pp. 15697–15715.
- Schaber, G.G., Strom, R.G., Moore, H.J., Soderblom, L.A., Kirk, R.L., Chadwick, D.J., Dawson, D.D., Gaddis, L.R., Boyce, J.M., and Russell, J., Geology and distribution of impact craters on Venus: What are they telling us?, *J. Geophys. Res.: Planets*, 1992, vol. 97, no. E8, pp. 13257–13301.
- Schmidt, R.M., Preliminary scaling results for crater rim-crest diameter, *Lunar and Planet. Sci. Conf. 18th*, 1987, pp. 878–879. <https://articles.adsabs.harvard.edu/pdf/1987LPI....18..878S>.
- Schmidt, R.M. and Housen, K.R., Some recent advances in the scaling of impact and explosion cratering, *Int. J. Impact Eng.*, 1987, vol. 5, nos. 1–4, pp. 543–560.
- Schulz, T., Koeberl, C., Luguët, A., van Acken, D., Mohr-Westheide, T., Ozdemir, S., and Reimold, W.U., New constraints on the Paleoproterozoic meteorite bombardment of the Earth-Geochemistry and Re-Os isotope signatures of spherule layers in the BARB5 ICDP drill core from the Barberton Greenstone Belt, South Africa, *Geochim. Cosmochim. Acta*, 2017, vol. 211, pp. 322–340.
- Schutt, D.L., Lowry, A.R., and Buehler, J.S., Moho temperature and mobility of lower crust in the western United States, *Geology*, 2018, vol. 46, no. 3, pp. 219–222.
- Senft, L.E. and Stewart, S.T., Modeling the morphological diversity of impact craters on icy satellites, *Icarus*, 2011, vol. 214, no. 1, pp. 67–81.
- Simonson, B.M. and Glass, B.B., Spherule layers records of ancient impacts, *Ann. Rev. Earth Planet. Sci.*, 2004, vol. 32, pp. 329–361.
- Steffen, R., Strykowski, G., and Lund, B., High-resolution Moho model for Greenland from EIGEN-6C4 gravity data, *Tectonophysics*, 2017, vols. 706–707, pp. 206–220.
- Stixrude, L. and Lithgow-Bertelloni, C., Thermodynamics of mantle minerals. II. Phase equilibria, *Geophys. J. Int.*, 2011, vol. 184, no. 3, pp. 1180–1213.
- Strom, R.G., Schaber, G.G., and Dawson, D.D., The global resurfacing of Venus, *J. Geophys. Res.*, 1994, vol. 99, no. E5, pp. 10899–10926.
- Thompson, S.L. and Lauson, H.S., Improvements in the Chart-D radiation hydrodynamic code. III: Revised analytical equation of state, *SC-RR-71 0714*, Albuquerque, NM: Sandia Laboratories, 1972.
- Trowbridge, A.J., Garde, A.A., Melosh, H.J., and Andronicos, C.L., iSALE numerical modeling of the Maniitsoq structure, West Greenland: A crustal-scale column of mechanical mixing reaching the Moho, *Lunar Planet. Sci. Conf. 48*, 2017, p. 2305. <https://www.hou.usra.edu/meetings/lpsc2017/pdf/2305.pdf>.
- Valter, A.A., Dobryansky, Y.P., Lasarenko, E.E., and Tarasyuk, V.K., Shock metamorphism of quartz and estimation of masses motion in the bases of Boltysch and Ilyinets astroblemes of the Ukrainian Shield, *Lunar and Planet. Sci. Conf. 13, Houston, TX*, 1982, pp. 819–820. <https://articles.adsabs.harvard.edu/pdf/1982LPI....13..819V>.
- Werner, S.C. and Ivanov, B.A., Exogenic dynamics, cratering, and surface ages, in *Treatise on Geophysics*, Schubert, G., Ed., Oxford: Elsevier, 2015, 2nd ed., ch. 10.10, pp. 327–365.
- Wünnemann, K., Collins, G.S., and Melosh, H.J., A strain-based porosity model for use in hydrocode simulations of impacts and implications for transient crater growth in porous targets, *Icarus*, 2006, vol. 180, no. 2, pp. 514–527.
- Yakymchuk, C., Kirkland, C.L., Cavosie, A.J., Szilas, K., Hollis, J., Gardiner, N.J., Waterton, P., Steinfeld, A., and Martin, L., Stirred not shaken; critical evaluation of a proposed Archean meteorite impact in West Greenland, *Earth Planet. Sci. Lett.*, 2021, vol. 557, p. 116730.

*Translated by E. Seifina*

**Publisher's Note.** Pleiades Publishing remains neutral with regard to jurisdictional claims in published maps and institutional affiliations.